# *Supplementary Material*

## 1 Supplementary Figures and Tables

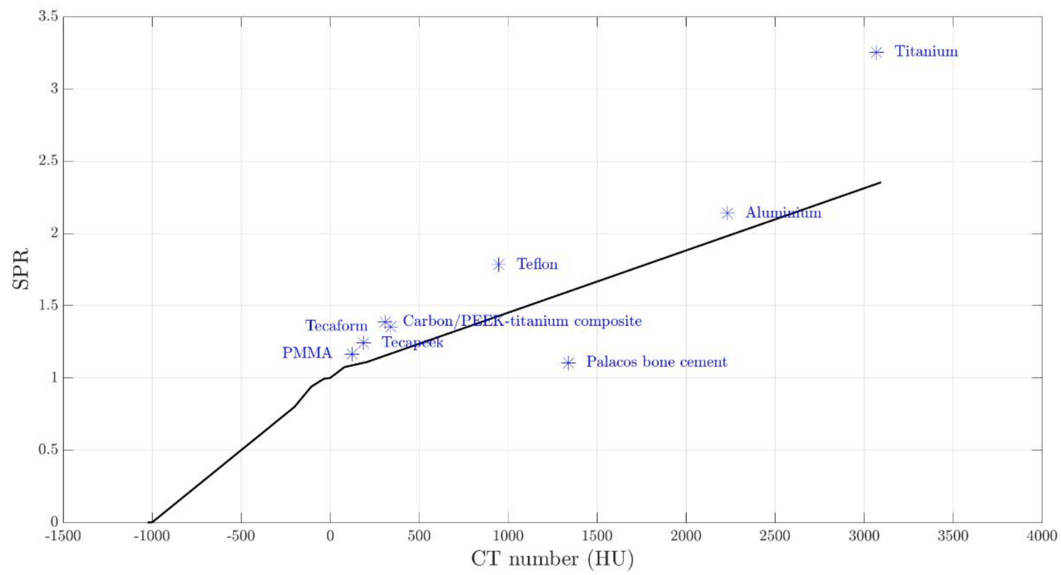


**Supplementary Figure 1.** Single-energy CT (SECT)-based CT-number-to-stopping-power-ratio (SPR) calibration curve, or Hounsfield look-up table (HLUT), together with the eight non-tissue implant materials used in this study.

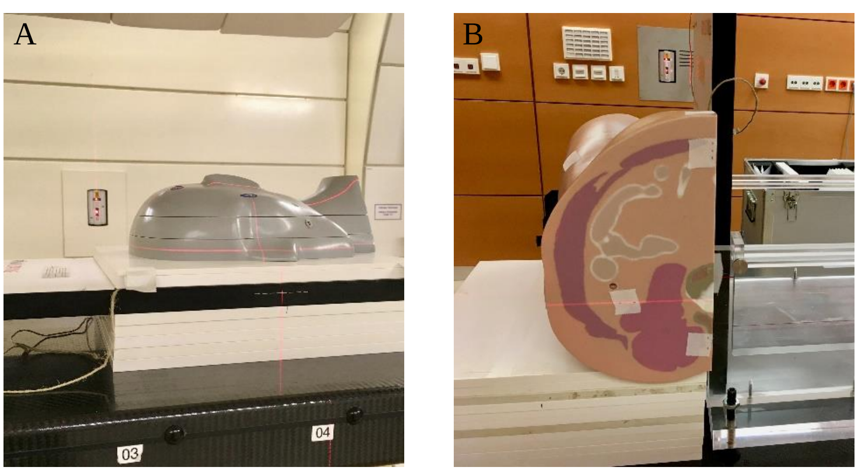


**Supplementary Figure 2.** Dosimetric measurements with anthropomorphic head and pelvic phantoms. For the head phantom (A), irradiation was performed using the gantry at an angle of 0° with the half-head phantom placed on top of the OCTAVIUS® detector. For the pelvic phantom (B), irradiation was performed using the horizontal beam line with the half-pelvic phantom placed in front of the OCTAVIUS® detector.

| Technical features | Dual-source CT | Dual-spiral | Fast tube voltage switching | Twin-beam | Dual-layer detector | Photon-counting CT |
|---|---|---|---|---|---|---|
| **Spectral mode** | spectral mode preselection, prospective results generation | spectral mode preselection, prospective results generation | spectral mode preselection, prospective results generation | spectral mode preselection, prospective results generation | no special mode, pro- and retrospective results generation | no special mode, pro- and retrospective results generation |
| **Acquisition mode** | dedicated dual-energy | dedicated dual-energy | dedicated dual-energy | dedicated dual-energy | implicit dual-energy | implicit multi-energy |
| **Temporal coherence** | high (quarter rotation angular offset) | low (large offset) | high (nearly perfect alignment) | medium (half collimation offset) | perfect alignment | perfect alignment |
| **Spatio-temporal resolution** | full capabilities | full capabilities | limited capabilities (impaired spatial resolution) | full capabilities | full capabilities | full capabilities (superior spatial resolution) |
| **Availability of dose modulation** | yes (individual tube current modulation) | yes (individual tube current modulation) | no (no tube current modulation) | yes (tube current modulation) | yes (tube current modulation) | yes (tube current modulation) |
| **Spectral separation** | very high (with additional tin filtration) | very high | medium (“smearing of spectra” due to finite kV-switching times) | low | medium | high |
| **Cross-scatter occurrence** | between source–detector systems | no | no | between detector rows (halves) separated by the system’s central vertical plane | between detector layers | no |
| **Field-of-view** | limited (up to 350 mm) | full | full | full | full | full |

| | | | | | | |
|---|---|---|---|---|---|---|
| **Time-resolved respiratory imaging** | feasible with phase matching in post-processing | feasible with phase matching in post-processing | feasible with phase matching in post-processing | feasible with phase matching in post-processing | no technical limitations | no technical limitations |
| **Contrast-enhanced imaging** | multi-phase (arterial and venous) | limited to late or delayed phase | multi-phase (arterial and venous) | limited to late or delayed phase | multi-phase (arterial and venous) | multi-phase (arterial and venous) |
| **Spectral decompo-sition** | image-based material decomposition | image-based material decomposition | projection-based material decomposition | image-based material decomposition | projection-based material decomposition | projection-based material decomposition |

**Supplementary Table 1.** Comparison of different dual-energy or spectral CT acquisition techniques with a focus on particle therapy treatment planning. Note that despite having the potential to provide spectral data, CT systems with energy-resolving, photon-counting detectors are just starting to become clinically available but do not yet see widespread use.

| | Dual-source CT | Dual-spiral | Fast tube voltage switching | Twin-beam | Dual-layer detector | Photon-counting CT |
|---|---|---|---|---|---|---|
| **Theoretical studies** | • [4] Bär et al (2017) | | | | | • [27] Taasti et al (2018) |
| **Phantom studies (phantoms with simplified geometries or anthropo-morphic phantoms)** | • [2] Almeida et al (2018)<br>• [4] Bär et al (2017)<br>• [5] Bär et al (2018)<br>• [7] Bourque et al (2014)<br>• [10] Hansen et al (2015)<br>• [11] Hudobivnik et al (2016)<br>• [12] Hünemohr et al (2014)<br>• [15] Li et al (2017)<br>• [17] Michalak et al (2017)<br>• [23] Saito et al (2017)<br>• [29] Wohlfahrt et al (2018) | • [1] Almeida et al (2017)<br>• [2] Almeida et al (2018)<br>• [8] Chacko et al (2021)<br>• [19] Mossahebi et al (2020)<br>• [24] Shen et al (2018)<br>• [33] Zhang et al (2019)<br>• [34] Zhu & Penfold (2016) | • [21] Ohira et al (2022) | • [2] Almeida et al (2018) | • [9] Faller et al (2020)<br>• [13] Landry et al (2019)<br>• [20] Ohira et al (2018) | • [14] Lee et al (2021) |
| **Biological tissue sample studies (homo-geneous or hetero-geneous tissue samples)** | • [5] Bär et al (2018)<br>• [18] Möhler et al (2018)<br>• [25] Taasti et al (2017) | • [25] Taasti et al (2017)<br>• [32] Xie et al (2018) | | • [25] Taasti et al (2017) | | • [27] Taasti et al (2018) |

| | | | | | | |
|---|---|---|---|---|---|---|
| **Patient studies** | • [6] Bär et al (2021)<br>• [11] Hudobivnik et al (2016)<br>• [26] Taasti et al (2018) | • [2] Almeida et al (2018)<br>• [22] Peters et al (2021)<br>• [26] Taasti et al (2018)<br>• [28] Wohlfahrt et al (2017)<br>• [30] Wohlfahrt et al (2018)<br>• [31] Wohlfahrt et al (2019) | | | • [3] Ates et al (2021)<br>• [16] Longarino et al (2022) | |

**Supplementary Table 2.** Selected publications of different dual-energy or spectral CT acquisition techniques currently available with a focus on particle therapy treatment planning. Note: The table is in alphabetical order and might not be exhaustive.

[1] Almeida et al (2017): Siemens SOMATOM Definition Open AS
[2] Almeida et al (2018): Siemens SOMATOM Force, Siemens SOMATOM Confidence RT Pro, Siemens SOMATOM Definition Edge
[3] Ates et al (2021): Philips IQon Spectral CT
[4] Bär et al (2017): Siemens SOMATOM Definition Flash
[5] Bär et al (2018): Siemens SOMATOM Definition Flash
[6] Bär et al (2021): Siemens SOMATOM Definition Flash
[7] Bourque et al (2014): Siemens SOMATOM Definition Flash
[8] Chacko et al (2021): Siemens SOMATOM Confidence RT Pro
[9] Faller et al (2020): Philips IQon Spectral CT
[10] Hansen et al (2015): Siemens SOMATOM Definition Flash
[11] Hudobivnik et al (2016): Siemens SOMATOM Force
[12] Hünemohr et al (2014): Siemens SOMATOM Definition Flash
[13] Landry et al (2019): Philips IQon Spectral CT
[14] Lee et al (2021): Energy-differentiation-type 64-channel cadmium telluride (CdTe) radiation line sensor module (C10413, Hamamatsu, Japan)
[15] Li et al (2015): Siemens SOMATOM Force
[16] Longarino et al (2022): Philips IQon Spectral CT
[17] Michalak et al (2017): Siemens SOMATOM Force
[18] Möhler et al (2018): Siemens SOMATOM Definition Flash
[19] Mossahebi et al (2020): Siemens SOMATOM Definition Edge
[20] Ohira et al (2018): Philips IQon Spectral CT
[21] Ohira et al (2022): GE Healthcare Revolution HD
[22] Peters et al (2021): Siemens SOMATOM Definition AS
[23] Saito et al (2017): Siemens SOMATOM Definition Flash
[24] Shen et al (2018): GE Healthcare LightSpeed QX/i
[25] Taasti et al (2017): Siemens SOMATOM Definition AS, Siemens SOMATOM Definition Flash, Siemens SOMATOM Force, Siemens SOMATOM Definition Edge
[26] Taasti et al (2018): Siemens SOMATOM Definition Flash, Philips Brilliance Big Bore
[27] Taasti et al (2018): Siemens research SOMATOM CounT
[28] Wohlfahrt et al (2017): Siemens SOMATOM Definition AS
[29] Wohlfahrt et al (2018): Siemens SOMATOM Definition AS
[30] Wohlfahrt et al (2018): Siemens SOMATOM Definition AS
[31] Wohlfahrt et al (2019): Siemens SOMATOM Definition AS
[32] Xie et al (2018): Siemens SOMATOM Sensation Open
[33] Zhang et al (2019): Philips Brilliance Big Bore
[34] Zhu & Penfold (2016): Philips Brilliance Big Bore

| Feature | Spectral CT 7500 | IQon Spectral CT |
|---|---|---|
| Generator power | 120 kW | 120 kW |
| Maximum detector collimation | 128 × 0.625 mm | 64 × 0.625 mm |
| Coverage (per rotation) | 80 mm | 40 mm |
| Minimum gantry rotation time | 0.27 s | 0.27 s |
| Maximum scannable range (axial) | 2000 mm | 2100 mm |
| Bore size | 800 mm | 700 mm |
| Conventional reconstruction time | iDose$^4$: 93% of reference protocols under 1 minute | iDose$^4$: majority of reference protocols under 1 minute |
| Spectral reconstruction time | 1–2 minutes for the majority of cases | 3–5 minutes for the majority of cases |
| Spectral temporal resolution | Simultaneous in the same time and space | Simultaneous in the same time and space |
| Spectral $kV_p$ stations | 100, 120, 140 | 120, 140 |

**Supplementary Table 3.** Comparison of the Philips Spectral CT 7500 [35] and IQon Spectral CT [36] scanners.

| Protocol | Tube voltage ($kV_p$) | Tube current-time product (mAs) | Colli-mation (mm) | Rotation time (s) | Pitch | $CTDI_{vol}$ (mGy) | Slice thickness and spacing (mm) | Recon-struction filter |
|---|---|---|---|---|---|---|---|---|
| Head | 120 | 300 | 64 × 0.625 | 0.5 | 0.8 | 47.2 | 1.5 | UB |
| Body | 120 | 300 | 128 × 0.625 | 0.5 | 0.8 | 23.2 | 2.0 | B |

**Supplementary Table 4.** Image acquisition settings and reconstruction parameters for head and body protocols.

| **Phantom** | **LC** | | | | **SC** | | | |
|---|---|---|---|---|---|---|---|---|
| Protocol | Head | Body | | | Head | Body | | |
| iDose$^4$ level | 0 | 0 | 3 | 6 | 0 | 0 | 3 | 6 |
| Mean overall relative residual | 0.728 | 0.725 | 0.723 | 0.724 | 0.761 | 0.613 | 0.579 | 0.605 |
| RMSE | 0.0086 | 0.0084 | 0.0085 | 0.0084 | 0.0089 | 0.0056 | 0.0056 | 0.0057 |
| $r$ | 0.9998 | 0.9998 | 0.9998 | 0.9998 | 0.9998 | 0.9998 | 0.9998 | 0.9998 |
| $\alpha$ | 1.016 | 1.011 | 1.011 | 1.001 | 1.015 | 1.005 | 1.005 | 1.005 |
| $\delta$ | –0.012 | –0.006 | –0.006 | –0.006 | –0.010 | –0.002 | –0.001 | –0.002 |

**Supplementary Table 5.** Accuracy of dual-layer spectral CT (DLCT)-based stopping power ratio (SPR) predictions across head and body protocols and iDose$^4$ levels 0, 3, and 6 for the LC (“long cylinder”) phantom and SC (“short cylinder”) phantom.

| **Phantom** | **LC** | | | | **SC** | | | |
|---|---|---|---|---|---|---|---|---|
| Protocol | Head | Body | | | Head | Body | | |
| iDose$^4$ level | 0 | 0 | 3 | 6 | 0 | 0 | 3 | 6 |
| Mean overall relative residual | 1.514 | 1.538 | 1.540 | 1.537 | 1.515 | 1.514 | 1.523 | 1.516 |
| RMSE | 0.0246 | 0.0255 | 0.0256 | 0.0256 | 0.0240 | 0.0243 | 0.0244 | 0.0243 |
| $r$ | 0.9958 | 0.9956 | 0.9956 | 0.9956 | 0.9959 | 0.9958 | 0.9958 | 0.9958 |
| $\alpha$ | 1.009 | 1.012 | 1.012 | 1.012 | 1.005 | 1.007 | 1.008 | 1.008 |
| $\delta$ | –0.009 | –0.009 | –0.009 | –0.009 | –0.007 | –0.008 | –0.008 | –0.008 |

**Supplementary Table 6.** Accuracy of single-energy CT (SECT)-based stopping power ratio (SPR) predictions across head and body protocols and iDose$^4$ levels 0, 3, and 6 for the LC (“long cylinder”) phantom and SC (“short cylinder”) phantom.

## 2 References

[1] Almeida IP, Landry G, Dedes G, Patel R, Pankuch M, Coutrakon G et al. Evaluating clinical stopping power estimation from a radiotherapy dual energy CT scanner. Acta Phys Pol B (2017) 48(10):1619-1623. doi:10.5506/APhysPolB.48.1619

[2] Almeida IP, Schyns LEJR, Vaniqui A, van der Heyden B, Dedes G, Resch AF et al. Monte Carlo proton dose calculations using a radiotherapy specific dual-energy CT scanner for tissue segmentation and range assessment. Phys Med Biol (2018) 63(11):115008. doi: 10.1088/1361-6560/aabb60

[3] Ates O, Hua CH, Zhao L, Shapira N, Yagil Y, Merchant TE et al. Feasibility of using post-contrast dual-energy CT for pediatric radiation treatment planning and dose calculation. Br J Radiol (2021) 94(1118):20200170. doi: 10.1259/bjr.20200170

[4] Bär E, Lalonde A, Royle G, Lu HM, Bouchard H. The potential of dual-energy CT to reduce proton beam range uncertainties. Med Phys (2017) 44(6):2332-2344. doi: 10.1002/mp.12215

[5] Bär E, Lalonde A, Zhang R, Jee KW, Yang K, Sharp G et al. Experimental validation of two dual-energy CT methods for proton therapy using heterogeneous tissue samples. Med Phys (2018) 45(1):48-59. doi: 10.1002/mp.12666

[6] Bär E, Collins-Fekete CA, Rompokos V, Zhang Y, Gaze MN, Warry A et al. Assessment of the impact of CT calibration procedures for proton therapy planning on pediatric treatments. Med Phys (2021) 48(9):5202-5218. doi: 10.1002/mp.15062

[7] Bourque AE, Carrier JF, Bouchard H. A stoichiometric calibration method for dual energy computed tomography. Phys Med Biol (2014) 59(8):2059-2088. doi: 10.1088/0031-9155/59/8/2059

[8] Chacko MS, Grewal HS, Wu D, Sonnad JR. Accuracy of proton stopping power estimation of silicone breast implants with single and dual-energy CT calibration techniques. J Appl Clin Med Phys (2021) 22(9):159-170. doi: 10.1002/acm2.13358

[9] Faller FK, Mein S, Ackermann B, Debus J, Stiller W, Mairani A. Pre-clinical evaluation of dual-layer spectral computed tomography-based stopping power prediction for particle therapy planning at the Heidelberg Ion Beam Therapy Center. Phys Med Biol (2020) 65(9):095007. doi: 10.1088/1361-6560/ab735e

[10] Hansen DC, Seco J, Sørensen TS, Petersen JB, Wildberger JE, Verhaegen F et al. A simulation study on proton computed tomography (CT) stopping power accuracy using dual energy CT scans as benchmark. Acta Oncol (2015) 54(9):1638-1642. doi: 10.3109/0284186X.2015.1061212

[11] Hudobivnik N, Schwarz F, Johnson T, Agolli L, Dedes G, Tessonnier T et al. Comparison of proton therapy treatment planning for head tumors with a pencil beam algorithm on dual and single energy CT images. Med Phys (2016) 43(1):495-504. doi: 10.1118/1.4939106

[12] Hünemohr N, Krauss B, Tremmel C, Ackermann B, Jäkel O, Greilich S. Experimental verification of ion stopping power prediction from dual energy CT data in tissue surrogates. Phys Med Biol (2014) 59(1):83-96. doi: 10.1088/0031-9155/59/1/83

[13] Landry G, Dörringer F, Si-Mohamed S, Douek P, Abascal JFPJ, Peyrin F et al. Technical Note: Relative proton stopping power estimation from virtual monoenergetic images reconstructed from dual-layer computed tomography. Med Phys (2019) 46(4):1821-1828. doi: 10.1002/mp.13404

[14] Lee SH, Sunaguchi N, Nagao A, Hirano Y, Sakurai H, Kano Y et al. Calculation of Stopping-Power Ratio from Multiple CT Numbers Using Photon-Counting CT System: Two- and Three-Parameter-Fitting Method. Sensors (2021) 21(4):1215. doi: 10.3390/s21041215

[15] Li B, Lee HC, Duan X, Shen C, Zhou L, Jia X et al. Comprehensive analysis of proton range uncertainties related to stopping-power-ratio estimation using dual-energy CT imaging. Phys Med Biol (2017) 62(17):7056-7074. doi: 10.1088/1361-6560/aa7dc9

[16] Longarino FK, Tessonnier T, Mein S, Harrabi SB, Debus J, Stiller W et al. Dual-layer spectral CT for proton, helium, and carbon ion beam therapy planning of brain tumors. J Appl Clin Med Phys (2022) 23(1):e13465. doi: 10.1002/acm2.13465

[17] Michalak G, Taasti V, Krauss B, Deisher A, Halaweish A, McCollough C. A comparison of relative proton stopping power measurements across patient size using dual- and single-energy CT. Acta Oncol (2017) 56(11):1465-1471. doi: 10.1080/0284186X.2017.1372625

[18] Möhler C, Russ T, Wohlfahrt P, Elter A, Runz A, Richter C et al. Experimental verification of stopping-power prediction from single- and dual-energy computed tomography in biological tissues. Phys Med Biol (2018) 63(2):025001. doi: 10.1088/1361-6560/aaa1c9

[19] Mossahebi S, Sabouri P, Chen H, Mundis M, O'Neil M, Maggi P et al. Initial Validation of Proton Dose Calculations on SPR Images from DECT in Treatment Planning System. Int J Part Ther (2020) 7(2):51-61. doi: 10.14338/IJPT-XX-000XX.1

[20] Ohira S, Washio H, Yagi M, Karino T, Nakamura K, Ueda Y et al. Estimation of electron density, effective atomic number and stopping power ratio using dual-layer computed tomography for radiotherapy treatment planning. Physica Medica (2018) 56:34-40. doi: 10.1016/j.ejmp.2018.11.008

[21] Ohira S, Imai Y, Koike Y, Ono S, Ueda Y, Miyazaki M et al. Evaluation of Stopping Power Ratio Calculation Using Dual-energy Computed Tomography With Fast Kilovoltage Switching for Treatment Planning of Particle Therapy. In Vivo (2022) 36(1):103-110. doi: 10.21873/invivo.12681

[22] Peters N, Wohlfahrt P, Hofmann C, Möhler C, Menkel S, Tschiche M et al. Reduction of clinical safety margins in proton therapy enabled by the clinical implementation of dual-energy CT for direct stopping-power prediction. Radiother Oncol (2021) 166:71-78. doi: 10.1016/j.radonc.2021.11.002

[23] Saito M, Sagara S. Simplified derivation of stopping power ratio in the human body from dual-energy CT data. Med Phys (2017) 44(8):4179-4187. doi: 10.1002/mp.12386

[24] Shen C, Li B, Chen L, Yang M, Lou Y, Jia X. Material elemental decomposition in dual and multi-energy CT via a sparsity-dictionary approach for proton stopping power ratio calculation. Med Phys (2018) 45(4):1491-1503. doi: 10.1002/mp.12796

[25] Taasti VT, Michalak GJ, Hansen DC, Deisher AJ, Kruse JJ, Krauss B et al. Validation of proton stopping power ratio estimation based on dual energy CT using fresh tissue samples. Phys Med Biol (2017) 63(1):015012. doi: 10.1088/1361-6560/aa952f

[26] Taasti VT, Muren LP, Jensen K, Petersen JBB, Thygesen J, Tietze A et al. Comparison of single and dual energy CT for stopping power determination in proton therapy of head and neck cancer. Phys Imaging Radiat Oncol (2018) 6:14-19. doi: 10.1016/j.phro.2018.04.002

[27] Taasti VT, Hansen DC, Michalak GJ, Deisher AJ, Kruse JJ, Muren LP et al. Theoretical and experimental analysis of photon counting detector CT for proton stopping power prediction. Med Phys (2018) 45(11):5186-5196. doi: 10.1002/mp.13173

[28] Wohlfahrt P, Möhler C, Stützer K, Greilich S, Richter C. Dual-energy CT based proton range prediction in head and pelvic tumor patients. Radiother Oncol (2017) 125(3):526-533. doi: 10.1016/j.radonc.2017.09.042

[29] Wohlfahrt P, Möhler C, Richter C, Greilich S. Evaluation of Stopping-Power Prediction by Dual- and Single-Energy Computed Tomography in an Anthropomorphic Ground-Truth Phantom. Int J Radiat Oncol Biol Phys (2018) 100(1):244-253. doi: 10.1016/j.ijrobp.2017.09.025

[30] Wohlfahrt P, Troost EGC, Hofmann C, Richter C, Jakobi A. Clinical Feasibility of Single-Source Dual-spiral 4D Dual-Energy CT for Proton Treatment Planning Within the Thoracic Region. Int J Radiat Oncol Biol Phys (2018) 102(4):830-840. doi: 10.1016/j.ijrobp.2018.06.044

[31] Wohlfahrt P, Möhler C, Troost EGC, Greilich S, Richter C. Dual-Energy Computed Tomography to Assess Intra- and Inter-Patient Tissue Variability for Proton Treatment Planning of Patients With Brain Tumor. Int J Radiat Oncol Biol Phys (2019) 105(3):504-513. doi: 10.1016/j.ijrobp.2019.06.2529

[32] Xie Y, Ainsley C, Yin L, Zou W, McDonough J, Solberg TD et al. Ex vivo validation of a stoichiometric dual energy CT proton stopping power ratio calibration. Phys Med Biol (2018) 63(5):055016. doi: 10.1088/1361-6560/aaae91

[33] Zhang S, Han D, Williamson JF, Zhao T, Politte DG, Whiting BR et al. Experimental implementation of a joint statistical image reconstruction method for proton stopping power mapping from dual-energy CT data. Med Phys (2019) 46(1):273-285. doi: 10.1002/mp.13287

[34] Zhu J, Penfold SN. Dosimetric comparison of stopping power calibration with dual-energy CT and single-energy CT in proton therapy treatment planning. Med Phys (2016) 43(6):2845-2854. doi: 10.1118/1.4948683

[35] Philips. Spectral CT 7500 (2021). URL: https://www.usa.philips.com/healthcare/product/728333/spectral-ct-7500-philips-all-new-spectral-detector-ct-750 [accessed November 22, 2021]

[36] Philips. IQon Spectral CT (2021). URL: https://www.usa.philips.com/healthcare/product/HCNOCTN284/iqon-spectral-ct-certainty-lives-in-layers [accessed November 22, 2021]